

# Direct Observation of Tunable Thermal Conductance at Solid/porous Crystalline Solid Interfaces Induced by Water Adsorbents

Guang Wang<sup>1#</sup>, Hongzhao Fan<sup>1#</sup>, Jiawang Li<sup>1</sup>, Zhigang Li<sup>1</sup> and Yanguang Zhou<sup>1\*</sup>

<sup>1</sup>*Department of Mechanical and Aerospace Engineering, The Hong Kong University of Science and Technology, Clear Water Bay, Kowloon, Hong Kong SAR*

## Abstract

Improving interfacial thermal transport is crucial for heat dissipation in systems. Here, we design a strategy by utilizing the water adsorption-desorption process in porous metal-organic frameworks (MOFs) to tune the interfacial heat transfer. We observe a changeable thermal conductance across the solid/porous MOFs interfaces owing to the dense water channel formed by the adsorbed water molecules in MOFs. Our experimental results show that the interfacial thermal conductance of Au/Cu<sub>3</sub>(BTC)<sub>2</sub> heterointerfaces is increased up to 7.1 folds by this strategy, where Cu<sub>3</sub>(BTC)<sub>2</sub> is a typical porous MOF and usually referred to as HKUST-1. Our molecular dynamics simulations further show that the surface tension of Au layer will cause the adsorbed water molecules in HKUST-1 to gather at the interfacial region. The dense water channel formed at the interfacial region can activate the high-frequency lattice vibrations and act as an additional thermal pathway, and then enhance heat transfer across the interfaces significantly. Our findings provide a new concept for tailoring thermal transport at the solid/porous MOFs heterointerfaces which will largely benefit MOF-related applications.

---

<sup>#</sup>These authors contribute equally. <sup>\*</sup>Author to whom all correspondence should be addressed. Email: [maeygzhou@ust.hk](mailto:maeygzhou@ust.hk)

## INTRODUCTION

The importance of cooling cannot be overstated, with its research extending from the hardware of the digital age (e.g., electronic cooling<sup>1,2</sup>) to the process of life (e.g., building cooling<sup>3,4</sup>). Recently, passive cooling using metal-organic frameworks (MOFs) has attracted considerable interest in the cooling of electronics<sup>5</sup>, solar panels<sup>6,7</sup> and buildings<sup>8</sup> owing to its eco-friendly nature and zero-electricity characteristic. The corresponding cooling performance strongly depends on the thermal conductivity of MOFs and interfacial thermal conductance (ITC) between the objectives and MOFs. Unfortunately, MOFs typically possess a low thermal conductivity below 2 W/mK at the room temperature<sup>9-11</sup>, and are therefore regarded as poor thermal conductors. Even worse, the adsorbed water molecules in MOFs may decrease the effective thermal conductivity further<sup>12-14</sup>. For example, Babaei *et al.* suggested that the thermal conductivity of MOF-199 (i.e., HKUST-1) can be reduced from 0.69 W/mK to 0.21 W/mK when water molecules are adsorbed<sup>12,15</sup>. Consequently, there is a small space to manipulate the intrinsic thermal transport properties of MOFs. Designing an effective interfacial heat dissipation channel across the objectives and MOFs may be the only feasible way to improve the corresponding cooling performance. Till now, interfacial engineering using adhesion layer<sup>16-18</sup>, nanostructures<sup>19-23</sup>, chemical modification<sup>24,25</sup> and self-assembled monolayer (SAM)<sup>26-30</sup> has been widely applied to enhance the ITC. While it is possible to synthesize or fabricate the buffer layers, atomically controlling the structures of buffer layers is challenging and strongly limits its applications.

In this work, we design a sustainable and controllable strategy by utilizing a water adsorption process in porous MOFs to manipulate the interfacial heat transfer between Au and the MOF-199 (i.e., HKUST-1). Our frequency-domain thermoreflectance (FDTR)<sup>31,32</sup> measurements and molecular dynamics (MD) simulations show that the ITC between Au and HKUST-1 can be improved from 5.3 MW/m<sup>2</sup>K to 37.5 MW/m<sup>2</sup>K (~7.1 times) via this strategy. The dense water channels formed by the adsorbed water molecules in HKUST-1 serve as

additional thermal pathways and enhances the thermal energy across the interfaces significantly. The vibrational transmission coefficient function calculated by the frequency domain direct decomposition method (FDDDM)<sup>33–35</sup> further demonstrates that the thermal energy can be easily dissipated from Au to the MOF with adsorbents owing to the bridge effect of the adsorbed water molecules. Our findings provide new insights into thermal transport across MOFs and the objectives, which will greatly benefit the performance of MOFs-related cooling applications.

## RESULTS

**Materials synthesis and characterization.** Here, we choose a typical MOF (HKUST-1, i.e., MOF-199) which is widely used in gas storage and sensing<sup>36</sup> as a representative to investigate. The HKUST-1 crystals were synthesized by a hydrothermal method<sup>13</sup> (see **Methods** for details). Our synthesized HKUST-1 crystals showed an octahedral structure with a typical size of  $\sim 200$   $\mu\text{m}$ , and the triangle (111) facet<sup>37</sup> of the crystals was observed (**Figure 1a**). The powder X-ray diffraction (PXRD) measurements indicated that the synthesized HKUST-1 crystals possessed a good crystallinity (**Figure 1b**), which agrees with our calculated XRD spectrum. The HKUST-1 crystals were then mounted on a silicon wafer with a Kapton tape, and an Au transducer layer with a thickness of  $\sim 100$  nm (see **supplementary information (SI) Note 1** and **Figure S1** for details) was sputtered onto the crystals. We used the focused ion beam (FIB)-SEM system to get the cross-section of the Au/HKUST-1 heterointerfaces. The transmission electron microscopy (TEM) image (**Figure 1c**) implied a clear and smooth interface between HKUST-1 and Au, where Au had good contact with the HKUST-1 crystal. The Au coated HKUST-1 crystals were activated in a vacuum oven to evacuate the adsorbed water molecules during the synthesis process first, and then immersed in deionized (DI) water for 40 mins. The Raman spectrum of the samples showed a redshift of the peak at  $229\text{ cm}^{-1}$  to  $175\text{ cm}^{-1}$  when the HKUST-1 crystal was soaked in water for 20 mins (**Figure 1d**), which was attributed to

the water molecules' coordination with Cu-Cu units. There was no further change in the Raman spectrum after prolonged soaking, which indicated that the HKUST-1 was fully saturated<sup>38</sup>. For activated samples, our FDTR measurements were conducted in a nitrogen environment to avoid water adsorption during the measurements. For samples with saturated water, the Au-coated HKUST-1 crystals were briefly dried by a compressed air flow to remove the remaining water film on the surface after being taken out from the DI water (see **Methods** for details).

**FDTR measurements.** We then characterized the thermal transport properties of Au/HKUST-1 heterointerfaces using an ultrafast optical pump-probe spectroscopy based on the FDTR. Here, Au also served as the transducer and was heated by the pump laser during the FDTR measurements. The schematic heat transfer model for the FDTR measurements is shown in the inset in **Figure 2**. For activated samples where all the water molecules were released, the heat generated by the pump laser was transferred from the Au layer to the HKUST-1 framework directly. For samples with saturated water, the thermal energy was dissipated from the Au layer to both the HKUST-1 framework and the adsorbed water. The corresponding thermal conductivity was observed to be reduced compared to that of the activated HKUST-1, which agrees well with other experiments<sup>20</sup> and simulations<sup>12,14</sup> (see **SI Figure S3** for details).

Then, high-quality Au/HKUST-1 heterointerfaces with flat and smooth surfaces (see **SI Figure S4** for details) were chosen in the FDTR measurements to ensure a good thermoreflectance response. The phase lag between the pump beam and the probe beam measured by a lock-in amplifier in our FDTR measurements was fitted using a heat diffusion model<sup>39,40</sup>. The thermal conductivity ( $\kappa$ ) of HKUST-1 and interfacial thermal conductance (ITC) between the Au layer and the HKUST-1 can be then determined. In the FDTR measurements, the intensity radius for the probe and the pump laser beams were 5  $\mu\text{m}$  and 3.6  $\mu\text{m}$ , respectively. The measured data were collected under a 10 times optical microscope. It is noted that  $\kappa$  and ITC are two independent parameters in our thermal diffusion fitting model as the sensitivities of these two parameters are quite different (see **SI Note 2** for details). **Figure**

2 shows one representative FDTR measurement at room temperature. The measured thermal conductivity of the activated HKUST-1 crystals and HKUST-1 crystals with saturated water at the room temperature were 0.742 W/mK and 0.416 W/mK, respectively, which agreed well with other measured values<sup>13</sup>. The thermal conductance of Au/HKUST-1 heterointerfaces was found to increase from 5.17 MW/m<sup>2</sup>K to 31.5 MW/m<sup>2</sup>K when HKUST-1 adsorbed saturated water.

In total, we have measured over one hundred Au/HKUST-1 heterointerface samples from six batches (see **SI Note 3** for details), and the mean ITC is shown in **Figure 3a**. For the activated samples, the measured ITC ranged from 3 to 8 MW/m<sup>2</sup>K. The average value was  $5.33 \pm 0.15$  MW/m<sup>2</sup>K based on the Gaussian fitting of all measurements. When HKUST-1 adsorbed saturated water molecules, the mean ITC between the Au and the HKUST-1 increased to  $21.66 \pm 15.82$  MW/m<sup>2</sup>K, which was four times higher than the activated samples. The maximum ITC was 37.9 MW/m<sup>2</sup>K for the sample with saturated water. Meanwhile, it is worth noting that the minimal ITC for the water-saturated sample is only 5.8 MW/m<sup>2</sup>K which is close to the value of the activated samples. This may be attributed to the weak surface tension of the Au layer, which makes the water molecules in HKUST-1 are not likely to be absorbed into the Au/HKUST-1 interfacial region. We emphasize that the Au layer in different Au/HKUST-1 heterointerfaces is different (see **SI Figure S5** for details), which results from a combination of factors such as impurities, surface roughness and the crystal orientation of the Au film. Therefore, the surface tension of Au in some Au/HKUST-1 heterointerfaces may be too weak to gather the water molecules at the interfacial region (see our simulation analysis below for details).

**Interfacial thermal conductance calculated using atomistic simulations.** We also investigated the thermal transport across the Au/HKUST-1 heterointerfaces via nonequilibrium molecular dynamics (NEMD) simulations (see **Methods** and **SI Note 4** for calculation details). We first calculated the ITC of Au/HKUST-1 heterointerfaces without absorbed water

molecules. The calculated ITC was  $4.20 \pm 0.57$  MW/m<sup>2</sup>K, which was close to our measured value of  $5.33 \pm 0.15$  MW/m<sup>2</sup>K (**Figure 3a**). The agreement of the ITC between experiments and simulations indicated that the interatomic interactions between the Au and the HKUST-1 were properly described in our MD simulations. We then studied the thermal transport across the Au/HKUST-1 heterointerfaces considering adsorbed water molecules. As discussed above, the structures of the Au layers in our Au/HKUST-1 heterointerfaces are different. It is known that the interaction between Au and water molecules strongly depends on the structure of Au<sup>41,42</sup>. Therefore, two sets of interatomic potentials are fitted to depict the strong and weak Au/HKUST-1 heterointerfaces by comparing our calculated ITC with the measured ITC. The detailed fitting procedure for the interatomic interactions can be found in **SI Note 4**.

For the models with strong Au-water molecule interactions, the ITC increased first and then saturated to  $\sim 35$  MW/m<sup>2</sup>K with the adsorbed water molecules. The ITC for the Au/HKUST-1 heterointerfaces with saturated water molecules agreed well with the upper value of our experimental measurements. For the models with weak Au-water molecule interactions, the ITC increased to a stable value of  $\sim 10$  MW/m<sup>2</sup>K when HKUST-1 absorbed saturated water molecules, which was close to the lower value of the experimental results. We next investigated the dynamic water adsorption process in Au/HKUST-1 heterointerface models. Water molecules were initially adsorbed in HKUST-1 randomly (the water adsorption process can be found in **SI Note 4**). During the relaxation period, the adsorbed water molecules were found to cluster in the cages of HKUST-1 or be adsorbed in the interface region (**Figure 3b**). The former behaviour was because of the long-range electrostatic interactions among water molecules and their thermal motion, which may affect the thermal transport properties of HKUST-1 considering adsorbed water molecules<sup>14</sup>. The latter one was resulted from the intrinsic interactions between water molecules and Au, which may largely increase the ITC of Au/HKUST-1 heterointerfaces.

**Underlying mechanisms.** We further calculated the transmission coefficient function of Au/HKUST-1 heterointerfaces with/without absorbed water molecules using FDDDM<sup>33–35</sup>. The transmission coefficient function quantitatively characterizes the thermal energy exchange capability of vibrations. Our results showed that the vibrational transmission coefficient was generally increased when the water molecules were absorbed into the systems (**Figures 4a** and **4b**). The transmission coefficient function for the heterointerfaces with strong Au-water molecule interactions was found to be larger than that with weak Au-water molecule interactions. This was because more water molecules were adsorbed into the interfacial region for the heterointerfaces with strong Au-water molecule interactions.

Meanwhile, vibrations with frequencies higher than 4 THz (i.e., the cut-off frequency of Au, **Figure 4c**) were found to contribute little to the ITC for the pristine Au/HKUST-1 heterointerfaces. When a large number of water molecules were adsorbed into the interfacial region (e.g., the density of adsorbed water molecules was higher than 0.5 g/cm), some vibrations with frequencies higher than 4 THz could also transport thermal energy across the heterointerfaces (**Figures 4a** and **4b**). This is because of the bridge effect resulting from the adsorbed water molecules in the interfacial region. To analyse the bridge effect, we calculated the vibrational density of states (VDOSs) of Au, HKUST-1, water molecules and HKUST-1 with water molecules (**Figure 4c**). While there is an overlap below 4 THz between the VDOS of Au and that of HKUST-1, their large mismatch implies that the heat transport from Au to HKUST-1 is inefficient. Consequently, the ITC of the pristine Au/HKUST-1 heterointerfaces is low. However, the overlap of the VDOS between Au and water molecules is broad and apparent (the inset of **Figure 4c**), which leads to an increased ITC when water molecules are adsorbed into the interface region (**Figures 3, 4a, and 4b**).

Before closing, we quantitatively characterized the thermal energy across heterointerfaces from the Au layer to water molecules and the HKUST-1 framework. **Figure 4d** showed the ITC contributions resulting from the two channels of Au/water molecules and Au/HKUST-1

framework. The density of the adsorbed water molecules was 0, 0.2 and 0.5 g/cm<sup>3</sup> in our Au/HKUST-1 heterointerfaces. We found that the ITC resulting from the Au/HKUST-1 framework channel was independent of the density of the adsorbed water molecules and almost a constant value of ~5 MW/m<sup>2</sup>K. The corresponding ITC spectrum also showed a weak dependence on the density of the adsorbed water molecules (SI Note 4). However, both the total ITC and ITC spectrum contributed by the channel of Au/water molecules increase significantly with the adsorbed water molecules (Figure 4d and SI Note 4). Our results reveal that the adsorbed water molecules do not hinder the thermal transport between Au and HKUST-1 and provide extra thermal pathways to dissipate heat from Au.

## CONCLUSIONS

In summary, we have designed a tunable strategy utilizing the adsorbed water in porous HKUST-1 to manipulate the thermal transport across Au/HKUST-1 interfaces. Our FDTR measurements showed that a maximum ITC ~37.9 MW/m<sup>2</sup>K could be achieved when saturated water molecules were adsorbed in HKUST-1, which was ~7.1 times higher than that (i.e., ~5.3 MW/m<sup>2</sup>K) of the activated Au/HKUST-1 heterointerfaces. Our NEMD simulations further demonstrated that this ITC enhancement was because of the bridge effect of the dense water channel at the Au/HKUST-1 interfacial region formed by adsorbed water molecules in HKUST-1. The dense water channel at the interfacial region could not only activate the high-frequency lattice vibrations, but also act as an additional thermal pathway. As a result, the thermal energy can be easily dissipated from Au to the HKUST-1 with adsorbents owing to the bridge effect of the dense water channel, which is further confirmed by our calculated vibrational transmission coefficient function. Our work here proposed a new strategy based on the water adsorption-desorption process in porous MOFs to manipulate the heat transfer across MOFs/solid interfaces, which is important for MOF-related cooling applications.



## METHODS

### Synthesis and characterization of Au/HKUST-1 heterointerfaces

The HKUST-1 crystals were synthesized by a hydrothermal method<sup>13</sup>. First, 5 g Benzene-1,3,5-tricarboxylic acid (Bidepharm, 98%) and 0.6 g oxalic acid dihydrate (Aladdin, 99.5%) were dissolved in a mixture of 100 mL EtOH (VWR, 96%) and 10 mL DMF (RCI Labscan Limited, 99.8%). The solution with 16.5 g  $\text{Cu}(\text{NO}_3)_2 \cdot 3\text{H}_2\text{O}$  (Aladdin, 99%) and 90 mL DI water was slowly added to the above linker solution. The resulting suspension was stirred for 1 hour to ensure its thorough mixing, and then sealed in a capped jar. The suspension was then put in an 80 °C pre-heated oven for 48 hours. A mixture of blue HKUST-1 crystals and the insoluble white precipitate was then formed, and the precipitate was removed by adding fresh ethanol and pipetting out the white suspension. This process might be repeated several times until pure HKUST-1 crystals were obtained. Finally, these HKUST-1 crystals were rinsed in ethanol for 12 hours and activated in a 150 °C vacuum oven for 20 hours.

The HKUST-1 crystals were then mounted on a silicon wafer with a Kapton tape, and an ~100 nm Au layer was sputtered on the crystals to form Au/HKUST-1 heterointerface samples (Discovery 18, Denton Vacuum). The surface morphology of Au/HKUST-1 heterointerfaces was characterized by scanning electron microscopy (SEM, JSM-6490 Jeol). The PXRD of HKUST-1 was also measured at room temperature by powder diffractometer X'pert Pro (PANalytical,  $\text{CuK}\alpha 1$  radiation,  $\lambda = 1.54056 \text{ \AA}$ ). A cross-section of Au/HKUST-1 heterointerfaces was prepared by FIB-SEM dual beam system (FEI Helios G4 UX) using a standard lift-out procedure with a final milling step. The thickness of the specimen was ~100 nm, and the bright field images of the specimen's cross-section were captured by scanning transmission electron microscopy (STEM, JEM-ARM200F JEOL). The Raman spectroscopy measurements were performed using a Raman spectrometer (InVia, Renishaw) with an excitation wavelength of 514 nm. For the activated samples, the measurements were conducted in a vacuum chamber to avoid the adsorption of moisture during the test.

## FDTR measurements

To avoid moisture adsorption during our FDTR measurements for the activated sample, the Au/HKUST-1 heterointerface specimen was mounted in a semi-sealed chamber (Instec) with a slow nitrogen flow. For each FDTR test, the  $1/e^2$  diameter of the pump laser was measured using the beam offset method and the laser spot was fitted by the Gaussian profiles<sup>43</sup>. Typically, the radius of the pump and probe laser were around  $3.6 \mu\text{m}$  and  $5 \mu\text{m}$ , respectively. The phase lag between the probe laser and pump laser was collected by the lock-in amplifier (HF2LI, Zurich), and fitted by the heat diffusion model to obtain the thermal properties. The FDTR lasers were swept across the samples' surface under the optical microscope to find the smooth and flat area for good thermorefectance. Each sample spot was swept five times to reduce the noise in experiments. Based on the sensitivity analysis, the thermal conductivity and the ITC between Au and HKUST-1 crystal could be determined at the same time (see **SI Note 2** for details). To measure the thermal properties of Au/HKUST-1 heterointerfaces with adsorbed water, the activated samples were immersed in DI water for 40 mins. The immersion time in our experiments was long enough for the HKUST-1 crystals to absorb saturated water, which was confirmed by the Raman measurements (**Figure 1d**) and other references<sup>13,38</sup>. Then, we applied the slow compression air flow to remove the water film on the Au/HKUST-1 samples which were taken out from the water. The thermal properties of Au/HKUST-1 samples with saturated water were measured in the room environment using FDTR.

## MD simulation

In this paper, the NEMD simulations were performed to investigate the thermal transport of the Au/HKUST-1 heterointerfaces considering water adsorption. All MD simulations were implemented by the Large-scale Atomic/Molecular Massively Parallel Simulator (LAMMPS) software<sup>44</sup>. The size of the simulation systems was  $5.2 \text{ nm} \times 5.2 \text{ nm} \times 41.2 \text{ nm}$ . To calculate the interfacial thermal conductance, a symmetrical model was used here. Au atoms were located two sides of the system, and the HKUST-1 frameworks with/without adsorbed water

molecules were in the middle region (see **SI Note 4** for details). The embedded atom method potential was used to describe the interactions among Au atoms. A forcefield developed based on first-principles calculations was applied to describe the interaction of the HKUST-1 framework<sup>45</sup>. The interactions among water molecules were depicted by the extended simple point charge model (SPC/E)<sup>46</sup>. Parameters extracted from the universal force field (UFF) were adopted to describe the interactions between Au and HKUST-1<sup>47</sup>. The interactions between Au and water molecules were fitted based on parameters from references<sup>48</sup> and our experimental measurements. The long-range electrostatic interactions were considered in our simulations and solved by the particle-particle-particle mesh Ewald summation method<sup>49</sup>.

During the MD simulations, the systems were first relaxed in an isothermal-isobaric ensemble and then a canonical ensemble to release the residual stress. Following, the NEMD simulations were implemented to calculate interfacial thermal conductance. Periodic boundary conditions were applied along both  $x$  and  $y$  directions. The fixed boundary condition was applied along  $z$  direction. The temperature gradient was then generated by Langevin thermostats. The heat sink and source were placed at two sides of the systems near the fixed atoms. The temperature of the heat source and sink was set as 350 K and 250 K, respectively. When the steady temperature gradient was built, the accumulative thermal energies  $\Delta E$  added or subtracted to the system by thermostats were recorded for 2.5 ns. The heat current  $Q$  across the interface was then calculated by linearly fitting the slope of  $\Delta E$  versus simulation time. The temperature difference  $\Delta T$  was obtained by linearly extrapolating the temperature distributions at two sides of the interface. The interfacial thermal conductance is  $ITC = Q/(\Delta T \cdot A)$ , where  $A$  is the cross-sectional area of the systems.

### **FDDDM calculations**

The interfacial spectral thermal conductance and the corresponding transmission coefficient function are calculated by the FDDDM method<sup>33-35</sup> which is in the framework of NEMD

simulations. During NEMD simulations, the heat current transferred across the interface can be calculated by

$$Q_{left \rightarrow right} = \sum_{i \in left} \sum_{j \in right} \left\langle \frac{\partial U_j}{\partial \vec{r}_i} \cdot \vec{v}_i - \frac{\partial U_i}{\partial \vec{r}_j} \cdot \vec{v}_j \right\rangle \quad (1)$$

where  $U$  represents the potential energy,  $\vec{v}_i$  is atomic velocity and  $\vec{r}_i$  is atomic position. The atomic velocity and position are recorded during the NEMD simulation. Then, the spectral heat current can be obtained via

$$Q(\omega) = \text{Re} \sum_{i \in left} \sum_{j \in right} \int_{-\infty}^{+\infty} \left\langle \frac{\partial U_j}{\partial \vec{r}_i} \Big|_{\tau} \cdot \vec{v}_i(0) - \frac{\partial U_i}{\partial \vec{r}_j} \Big|_{\tau} \cdot \vec{v}_j(0) \right\rangle e^{i\omega\tau} d\tau \quad (2)$$

Since the potential used to depict the interface is a two-body interaction, the spectral heat current can be simplified into

$$Q(\omega) = 2 \text{Re} \sum_{i \in left} \sum_{j \in right} \int_{-\infty}^{+\infty} \vec{F}_{ij} \cdot \vec{v}_i(0) e^{i\omega\tau} d\tau \quad (3)$$

where the  $\vec{F}_{ij}$  is the interatomic force from atom  $j$  exerted on atom  $i$ .

Once the frequency-dependent heat current is obtained, the phonon transmission function can be then estimated based on the Landauer theory<sup>50-52</sup>. In the Landauer theory, the heat current spectrum from the left lead to the right lead through a junction connecting two leads at two different equilibrium heat-bath temperatures (i.e.,  $T_L$  and  $T_R$ ) is written in the form of

$$Q(\omega) = \hbar\omega [n_L(\omega) - n_R(\omega)] \Gamma(\omega) \quad (4)$$

where  $n$  is the equilibrium phonon distribution function at heat-bath temperatures and has the classical limit form of  $n_{L \text{ or } R}(\omega) = k_B T_{L \text{ or } R} / \hbar\omega$  in molecular dynamics simulations, in which  $\Gamma(\omega)$  is the phonon transmission function. The spectral thermal conductance  $G(\omega)$  is then written as

$$G(\omega) = \frac{\hbar\omega [n_L(\omega) - n_R(\omega)] \cdot \Gamma(\omega)}{S(T_L - T_R)} = \frac{\hbar\omega \Delta n(\omega) \cdot \Gamma(\omega)}{S \Delta T} \approx \frac{\hbar\omega \partial n(\omega) \cdot \Gamma(\omega)}{S \partial T} \stackrel{\text{classical limit}}{\approx} \frac{k_B \Gamma(\omega)}{S} \quad (5)$$

It should be noted that **Eq. (5)** is only valid when the temperature gradient is kept in the linear regime. Therefore, the phonon transmission function in NEMD simulations can be calculated using  $\Gamma(\omega) = Q(\omega) / k_B \Delta T$ .

## **Acknowledgments**

Y.Z. thanks the Equipment Competition fund (REC20EGR14) and the Sustainable and Smart Campus as a living lab fund (FS105) from the Hong Kong University of Science and Technology (HKUST), the open fund from the State Key Laboratory of Clean Energy Utilization (ZJUCEU2022009) and the ASPIRE Seed Fund (ASPIRE2022#1) from the ASPIRE League. Y.Z. also thanks for the Hong Kong SciTech Pioneers Award from the Y-LOT Foundation. The authors are grateful to the Materials Characterization and Preparation Facility (MCPF) of HKUST for their assistance in experimental characterizations.

## **Author contributions**

Y.Z. conceived the idea; Z.L. and Y.Z. supervised the project; G.W. designed the experiments and conducted the material synthesis, characterization, and performance investigation; H.F. did the calculations; J.L. conducted the characterization; G.W., F.H. and Y.Z. prepared the manuscript.; G.W., H.F., Z.L. and Y.Z. reviewed and revised the manuscript.

## **Supplementary information**

The online version contains supplementary information is available.

## References

1. van Erp, R., Soleimanzadeh, R., Nela, L., Kampitsis, G. & Matioli, E. Co-designing electronics with microfluidics for more sustainable cooling. *Nature* **585**, 211–216 (2020).
2. Cho, J. & Goodson, K. E. Cool electronics. *Nat. Mater.* **14**, 136–137 (2015).
3. Wang, S. *et al.* Scalable thermochromic smart windows with passive radiative cooling regulation. *Science* **374**, 1501–1504 (2021).
4. Wang, H. & Chen, Q. Impact of climate change heating and cooling energy use in buildings in the United States. *Energy Build.* **82**, 428–436 (2014).
5. Wang, C. *et al.* A Thermal Management Strategy for Electronic Devices Based on Moisture Sorption-Desorption Processes. *Joule* **4**, 435–447 (2020).
6. Cheng, P. *et al.* Advanced phase change hydrogel integrating metal-organic framework for self-powered thermal management. *Nano Energy* **105**, 108009 (2023).
7. Wang, G., Li, Y., Qiu, H., Yan, H. & Zhou, Y. High-performance and wide relative humidity passive evaporative cooling utilizing atmospheric water. *Droplet* **2**, e32 (2023).
8. Qin, M., Feaugas, O. & Zu, K. Novel metal-organic framework (MOF) based phase change material composite and its impact on building energy consumption. *Energy Build.* **273**, 112382 (2022).
9. B. Gunatilleke, W. D. C. *et al.* Thermal conductivity of a perovskite-type metal–organic framework crystal. *Dalton Trans.* **46**, 13342–13344 (2017).
10. Erickson, K. J. *et al.* Thin Film Thermoelectric Metal–Organic Framework with High Seebeck Coefficient and Low Thermal Conductivity. *Adv. Mater.* **27**, 3453–3459 (2015).
11. Huang, B. L. *et al.* Thermal conductivity of a metal-organic framework (MOF-5): Part II. Measurement. *Int. J. Heat Mass Transf.* **50**, 405–411 (2007).
12. Babaei, H. & Wilmer, C. E. Mechanisms of Heat Transfer in Porous Crystals Containing Adsorbed Gases: Applications to Metal-Organic Frameworks. *Phys. Rev. Lett.* **116**, 025902 (2016).
13. Babaei, H. *et al.* Observation of reduced thermal conductivity in a metal-organic framework due to the presence of adsorbates. *Nat. Commun.* **11**, 4010 (2020).
14. Fan, H., Yang, C. & Zhou, Y. Ultralong mean free path phonons in HKUST-1 and their scattering by water adsorbates. *Phys. Rev. B* **106**, 085417 (2022).
15. Babaei, H., H. McGaughey, A. J. & E. Wilmer, C. Effect of pore size and shape on the thermal conductivity of metal-organic frameworks. *Chem. Sci.* **8**, 583–589 (2017).
16. Jeong, M. *et al.* Enhancement of Thermal Conductance at Metal-Dielectric Interfaces Using Subnanometer Metal Adhesion Layers. *Phys. Rev. Appl.* **5**, 014009 (2016).
17. Sandell, S. *et al.* Enhancement of Thermal Boundary Conductance of Metal–Polymer System. *Nanomaterials* **10**, 670 (2020).
18. Chang, G. *et al.* Regulated Interfacial Thermal Conductance between Cu and Diamond by a TiC Interlayer for Thermal Management Applications. *ACS Appl. Mater. Interfaces* **11**, 26507–26517 (2019).
19. Xu, Y., Wang, G. & Zhou, Y. Broadly manipulating the interfacial thermal energy transport across the Si/4H-SiC interfaces via nanopatterns. *Int. J. Heat Mass Transf.* **187**, 122499 (2022).

20. Lee, E., Zhang, T., Yoo, T., Guo, Z. & Luo, T. Nanostructures Significantly Enhance Thermal Transport across Solid Interfaces. *ACS Appl. Mater. Interfaces* **8**, 35505–35512 (2016).
21. Tian, Z., Esfarjani, K. & Chen, G. Enhancing phonon transmission across a Si/Ge interface by atomic roughness: First-principles study with the Green's function method. *Phys. Rev. B* **86**, 235304 (2012).
22. Goicochea, J. V., Hu, M., Michel, B. & Poulikakos, D. Surface Functionalization Mechanisms of Enhancing Heat Transfer at Solid-Liquid Interfaces. *J. Heat Transf.* **133**, (2011).
23. Cheng, Z. *et al.* Tunable Thermal Energy Transport across Diamond Membranes and Diamond–Si Interfaces by Nanoscale Graphoepitaxy. *ACS Appl. Mater. Interfaces* **11**, 18517–18527 (2019).
24. Foley, B. M. *et al.* Modifying Surface Energy of Graphene via Plasma-Based Chemical Functionalization to Tune Thermal and Electrical Transport at Metal Interfaces. *Nano Lett.* **15**, 4876–4882 (2015).
25. Hopkins, P. E. *et al.* Manipulating Thermal Conductance at Metal–Graphene Contacts via Chemical Functionalization. *Nano Lett.* **12**, 590–595 (2012).
26. Xu, B. *et al.* Weaker bonding can give larger thermal conductance at highly mismatched interfaces. *Sci. Adv.* **7**, eabf8197 (2021).
27. Fan, H. *et al.* Enhancement of Interfacial Thermal Transport between Metal and Organic Semiconductor Using Self-Assembled Monolayers with Different Terminal Groups. *J. Phys. Chem. C* **124**, 16748–16757 (2020).
28. O'Brien, P. J. *et al.* Bonding-induced thermal conductance enhancement at inorganic heterointerfaces using nanomolecular monolayers. *Nat. Mater.* **12**, 118–122 (2013).
29. Losego, M. D., Grady, M. E., Sottos, N. R., Cahill, D. G. & Braun, P. V. Effects of chemical bonding on heat transport across interfaces. *Nat. Mater.* **11**, 502–506 (2012).
30. Zheng, K. *et al.* Enhancing the Thermal Conductance of Polymer and Sapphire Interface via Self-Assembled Monolayer. *ACS Nano* **10**, 7792–7798 (2016).
31. Schmidt, A. J., Cheaito, R. & Chiesa, M. A frequency-domain thermoreflectance method for the characterization of thermal properties. *Rev. Sci. Instrum.* **80**, 094901 (2009).
32. Malen, J. A. *et al.* Optical Measurement of Thermal Conductivity Using Fiber Aligned Frequency Domain Thermoreflectance. *J. Heat Transf.* **133**, (2011).
33. Zhou, Y. & Hu, M. Full quantification of frequency-dependent interfacial thermal conductance contributed by two- and three-phonon scattering processes from nonequilibrium molecular dynamics simulations. *Phys. Rev. B* **95**, 115313 (2017).
34. Zhou, Y. & Hu, M. Quantitatively analyzing phonon spectral contribution of thermal conductivity based on nonequilibrium molecular dynamics simulations. II. From time Fourier transform. *Phys. Rev. B* **92**, 195205 (2015).
35. Sääskilähti, K., Oksanen, J., Tulkki, J. & Volz, S. Role of anharmonic phonon scattering in the spectrally decomposed thermal conductance at planar interfaces. *Phys. Rev. B* **90**, 134312 (2014).
36. H. Hendon, C. & Walsh, A. Chemical principles underpinning the performance of the metal–organic framework HKUST-1. *Chem. Sci.* **6**, 3674–3683 (2015).



37. Hashimoto, M., Okajima, S., Kondo, T., Hara, K. & Chun, W.-J. Thin Film Structures of Metal-Organic Framework [Cu<sub>3</sub>(BTC)<sub>2</sub>(H<sub>2</sub>O)<sub>3</sub>]<sub>n</sub> on TiO<sub>2</sub>(110). *Electrochemistry* **82**, 335–337 (2014).
38. Jeong, N. C., Samanta, B., Lee, C. Y., Farha, O. K. & Hupp, J. T. Coordination-Chemistry Control of Proton Conductivity in the Ionic Metal–Organic Framework Material HKUST-1. *J. Am. Chem. Soc.* **134**, 51–54 (2012).
39. Yang, J., Maragliano, C. & Schmidt, A. J. Thermal property microscopy with frequency domain thermorefectance. *Rev. Sci. Instrum.* **84**, 104904 (2013).
40. Cahill, D. G. Analysis of heat flow in layered structures for time-domain thermorefectance. *Rev. Sci. Instrum.* **75**, 5119–5122 (2004).
41. Wu, C.-D., Kuo, L.-M., Lin, S.-J., Fang, T.-H. & Hsieh, S.-F. Effects of temperature, size of water droplets, and surface roughness on nanowetting properties investigated using molecular dynamics simulation. *Comput. Mater. Sci.* **53**, 25–30 (2012).
42. Smith, T. The hydrophilic nature of a clean gold surface. *J. Colloid Interface Sci.* **75**, 51–55 (1980).
43. Feser, J. P. & Cahill, D. G. Probing anisotropic heat transport using time-domain thermorefectance with offset laser spots. *Rev. Sci. Instrum.* **83**, 104901 (2012).
44. Plimpton, S. Fast Parallel Algorithms for Short-Range Molecular Dynamics. *J. Comput. Phys.* **117**, 1–19 (1995).
45. Zhao, L. *et al.* A force field for dynamic Cu-BTC metal-organic framework. *J. Mol. Model.* **17**, 227–234 (2011).
46. Berendsen, H. J. C., Grigera, J. R. & Straatsma, T. P. The missing term in effective pair potentials. *J. Phys. Chem.* **91**, 6269–6271 (1987).
47. Rappe, A. K., Casewit, C. J., Colwell, K. S., Goddard, W. A. I. & Skiff, W. M. UFF, a full periodic table force field for molecular mechanics and molecular dynamics simulations. *J. Am. Chem. Soc.* **114**, 10024–10035 (1992).
48. Hu, H. & Sun, Y. Effect of nanopatterns on Kapitza resistance at a water-gold interface during boiling: A molecular dynamics study. *J. Appl. Phys.* **112**, 053508 (2012).
49. *Computer Simulation Using Particles*. (CRC Press, 2021). doi:10.1201/9780367806934.
50. Wang, J. & Wang, J.-S. Carbon nanotube thermal transport: Ballistic to diffusive. *Appl. Phys. Lett.* **88**, 111909 (2006).
51. Yamamoto, T., Konabe, S., Shiomi, J. & Maruyama, S. Crossover from Ballistic to Diffusive Thermal Transport in Carbon Nanotubes. *Appl. Phys. Express* **2**, 095003 (2009).
52. Rego, L. G. C. & Kirczenow, G. Quantized Thermal Conductance of Dielectric Quantum Wires. *Phys. Rev. Lett.* **81**, 232–235 (1998).

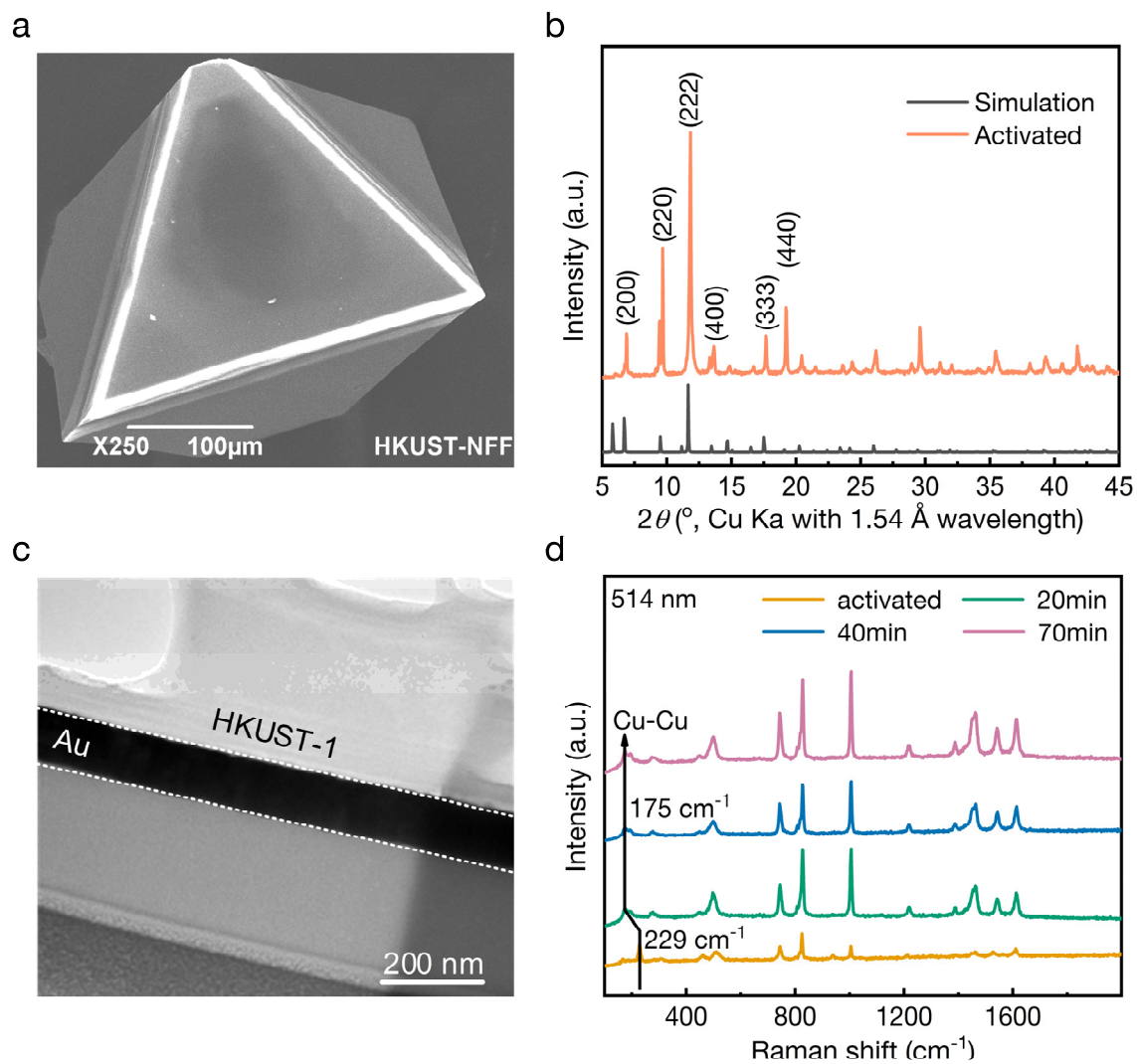


**Figure 1 Characterization of HKUST-1.** **a.** The SEM image of HKUST-1 single crystal after activation. **b.** The PXRD of HKUST-1 crystals after activation. **c.** A cross-section TEM image of Au/HKUST-1 heterointerfaces prepared by FIB-SEM. **d.** The Raman spectra of Au-coated HKUST-1 crystals after activation and immersed in water for 20 min, 40 min, and 70 min.

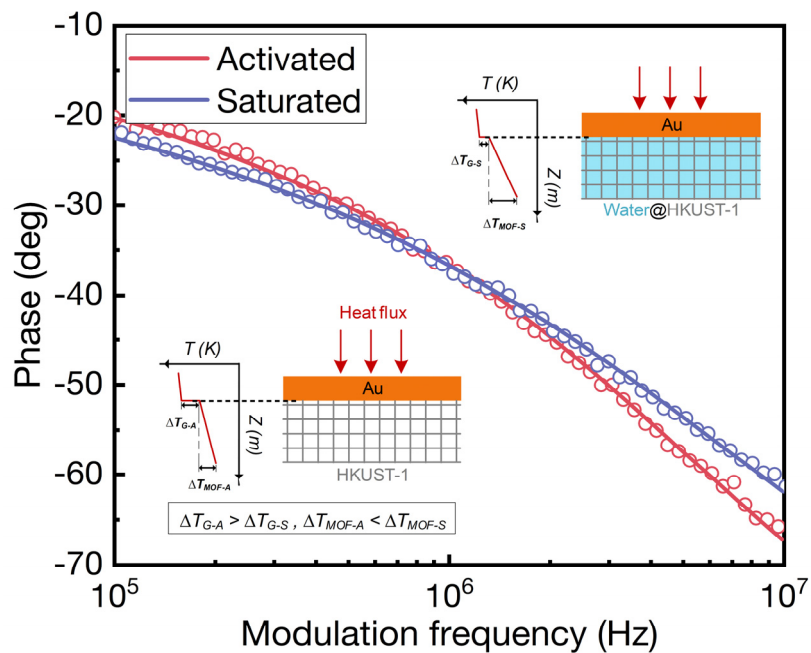


**Figure 2 Heat transport measurement with FDTR.** A representative FDTR signal phase as a function of the pump modulation frequency for the activated and fully saturated samples. The circle line is the raw data of FDTR measurements, and the solid line is the best-fitting line by the least square method. The inset picture on the bottom left is a schematic and corresponding temperature profiles of activated Au/HKUST-1 heterointerfaces, and the top right inset picture is for the sample with saturated water molecules.

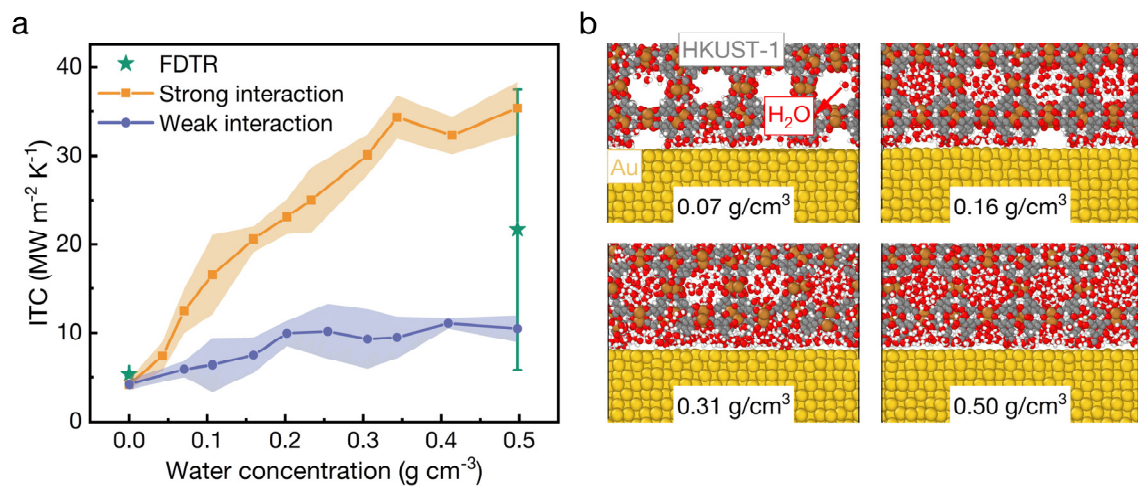


**Figure 3** The experimental and simulation results of phonon transport across Au/HKUST-1 heterointerfaces. **a.** The interfacial thermal conductance (ITC) of Au/HKUST-1 heterointerfaces considering adsorbed water molecules. **b.** The atomistic Au/HKUST-1 heterointerfaces with various adsorbed water molecules.

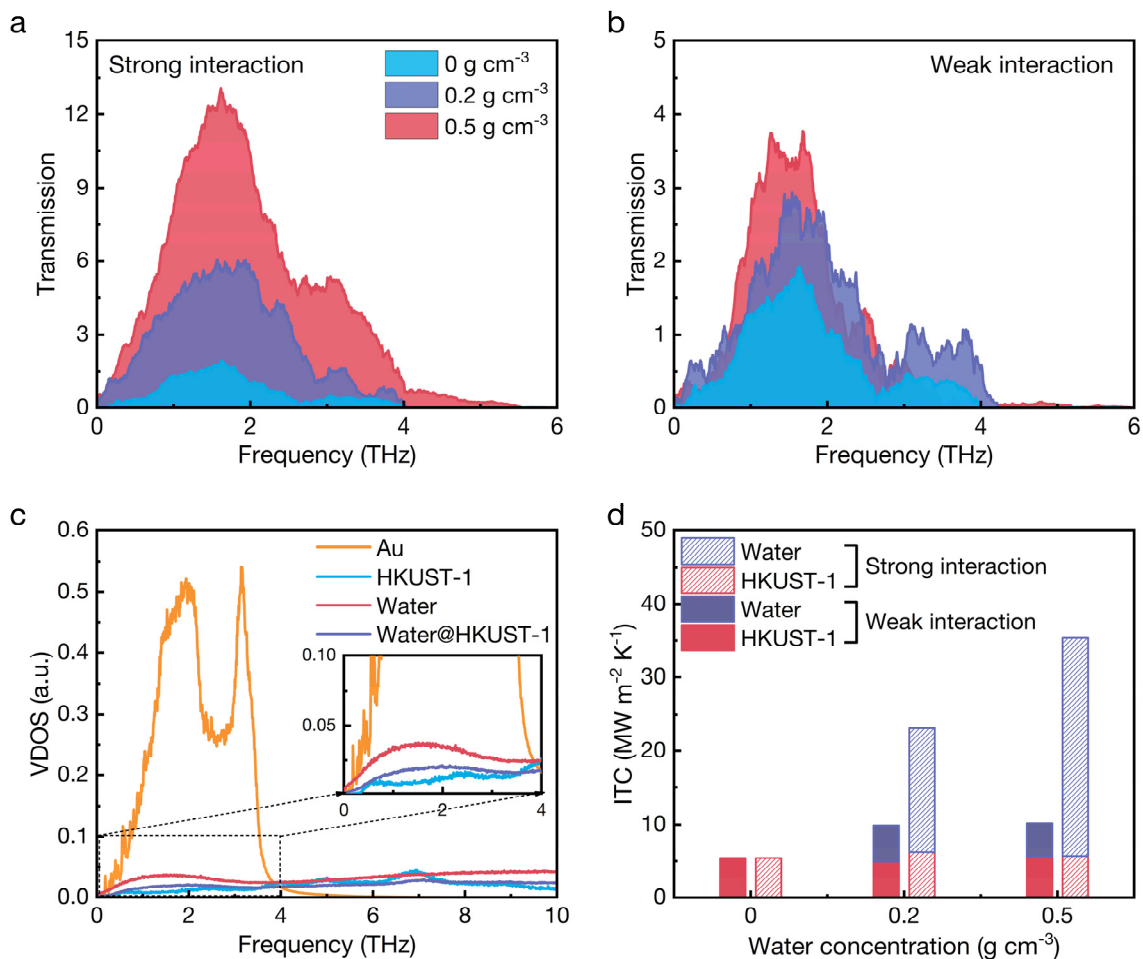


**Figure 4** The calculated thermal transport properties across **Au/HKUST-1 heterointerfaces**. **a.** The transmission coefficient function for the heterointerfaces with strong Au-water molecule interactions. **b.** The transmission coefficient function for the heterointerfaces with weak Au-water molecule interactions. **c.** The VDOSs of Au, HKUST-1, water molecules and HKUST-1 with water molecules. **d.** The interfacial thermal conductance (ITC) resulted from the two channels of Au/water molecules and Au/HKUST-1 framework. The density of adsorbed water molecules in HKUST-1 is 0, 0.2 and 0.5 g/cm<sup>3</sup>.